PSFC/RR-13-9

Variable Energy Acceleration in a Single Iron-Free Synchrocyclotron.

Radovinsky, A.L., Minervini, J.V., Michael P.C., Bromberg, L.,
Miller, C.E.

September 5, 2013

Plasma Science and Fusion Center
Massachusetts Institute of Technology
Cambridge MA 02139 USA

This work was supported by the U.S. Defense Threat Reduction Agency (DRTA), Grant No. HDTRA-09-1-00042.

Variable Energy Acceleration in a Single Iron-Free Synchrocyclotron

Alexey Radovinsky, Joseph Minervini, Phil Michael, Leslie Bromberg, Craig Miller

Abstract

Cyclotrons are used for high-energy particle production. Cyclotron technology has been developed over many decades, and today it is considered a mature technology. The present approach for making cyclotrons includes the use of magnetic iron poles and iron return yokes, to shape the magnetic field in the beam acceleration area and to magnetically shield the vicinity of the accelerator magnet from its high magnetic field. The latter is essential for medical cyclotrons used for patient treatment via proton radiotherapy, especially when the cyclotron is close to the patient, and also for cyclotrons used for the manufacturing of isotopes, which operate in close proximity to medical technicians.

A new, iron-free, design using high-field, high-current superconducting coils is proposed. Compared with the traditional design, with the iron yoke this approach leads to a significant weight reduction and a much more effective means of magnetic shielding. This simplifies its integration with the traditional applications and also presents new features, such as portability, possibility of using these cyclotrons on mobile platforms, ease of tuning in mass production and modular design arrangements.

An additional advantageous feature facilitated by the development of iron-free synchrocyclotrons is the capacity for energy variation and for using variable accelerated particles. Changing the energy of the beam is made possible by a proportional variation of the current in the superconducting coils. The implementation of this feature also requires several modifications to the design of cyclotron subsystems, e.g. ion source, RF and beam extraction. Variation of the beam energy is particularly important for the proton radiotherapy. It permits the longitudinal scanning of the beam delivered to the tumor in addition to the lateral scattering available by the contemporary state of the art.

1. Introduction

The two most common types of cyclotrons are referred to as isochronous cyclotrons and synchrocyclotrons. For both types, the ion beam is injected near the center of the device. The beam is confined by a magnetic field and is accelerated over many spiral orbits, before being extracted at a fixed radius near the edge of the device. In an isochronous cyclotron the radio frequency drive used to accelerate the beam is set to a fixed value, whereas in a synchrocyclotron the radio frequency drive varies to accommodate the relativistic mass increase in the beam at high energy. A second distinction between the two types is that a different magnetic field configuration is used for each type of cyclotron. The average magnetic field in an isochronous cyclotron increases with radial distance from the center of the machine towards the extraction radius to accommodate the relativistic mass increase in the beam, whereas in a synchrocyclotron

the magnetic field decreases from the center of the machine towards the extraction radius. The decline of the field with the radius in the synchrocyclotrons provides a weak focusing of the beam whereas in the isochronous cyclotrons a strong focusing method is used employing the azimutal variation of the magnetic field.

The conventional [1] approach to the design of synchrocyclotrons combines a single pair of high field superconducting coils with a massive ferromagnetic yoke and ferromagnetic pole pieces that generate, shape, and confine the cyclotron field. Figure 1 depicts the layout of the high-field synchrocyclotron, k250, designed by MIT for medical proton radiotherapy [2]. A split pair of superconducting coils produces magnetic field at the mid-plane as well as stray fields away from the cyclotron. The beam chamber is located at the midplane of the machine. The magnetic yokes and poles are used to increase the magnetic field at the midplane of the device, and to shape the field in this region, while the outer return iron yoke shields the magnetic field away from the machine. The fingers formed by the iron are used to shape the magnetic field in the beam extraction region.

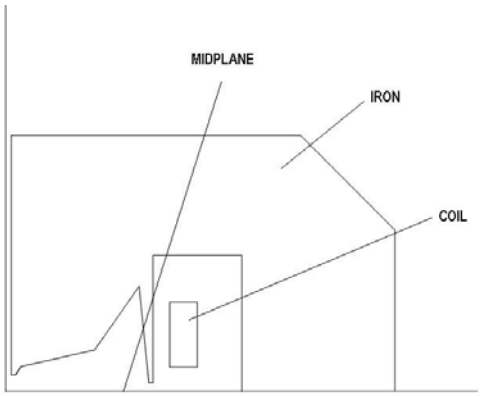

Fig. 1 Diagram of ¼ model of k250

Yoke-free isochronous cyclotron concepts have been proposed in the past. The field shaping for these isochronous cyclotrons was achieved using a combination of solenoids and either iron pole tips in the bore of the device [3], or bean-shaped coils above and below the beam chamber [4,5]. Solenoids created the background field and the adjusted the isochronous field profile, whereas the pole pieces or bean-shaped coils served to create the azimuthally varying field (AVF) ripple needed for beam stability. There was no mention of any means to vary the beam energy for any of these concepts and only Subotic [4] mentions a method for minimizing the stray magnetic field surrounding the device.

Recent studies conducted at the Technology and Engineering Department of the PSFC at MIT resulted in the development of an innovative concept for iron-free cyclotrons [6]. This design proposes the use of superconducting coils both for magnetic shielding of cyclotrons, as well as for generating the field profiles required for either isochronous cyclotrons or for synchrocyclotrons. A typical coil layout of an iron-free synchrocyclotron is shown in Fig. 2.

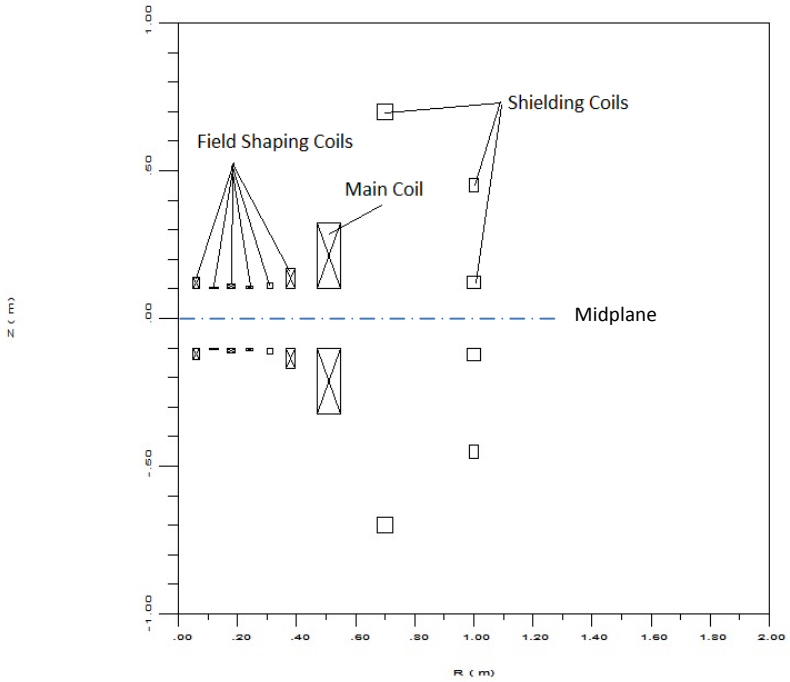

Fig. 2 Diagram of ½ coil model of an iron-free synchrocyclotron

Three sets of split pairs of coils produce the same functionality as the combination of the coils and the iron in the conventional design. The main coil creates the elevated background field in the beam chamber area. The B(r) profile of this background field does not provide the required weak beam focusing. A set of field shaping coils is used to adjust the field in the beam acceleration area to satisfy the weak focusing requirements. And finally, a set of shielding coils with the opposite currents reduces the stray fields in the vicinity of the cyclotron. Analyses [6] show that the shielding capacity of the shielding coils is far superior to the shielding by the return iron yoke in the conventional design. This approach to the magnetic shielding is similar to the general practice of the MRI technology [7]. In fact, the proposed magnetic shielding of the cyclotrons can be viewed as extending the methods used in the MRI magnet technology into the area of the cyclotron magnet design.

Other advantages of the iron-free cyclotrons are relatively light weight, and consequently portability, better compatibility with the on-gantry [8] or modular design, as well as ease of tuning in mass production.

A very attractive feature that is enabled by the development of iron-free approach is the possibility of the beam energy variation. This feature is essential [9] for providing a capability of the 3D irradiation of the tumor during a single treatment session by means of proton radiotherapy. Changing the energy of the beam requires several modifications to the cyclotron operation, some of which are enabled by the use of iron-free machines. Changing the energy of the beam, while maintaining the same extraction radius, requires a change in the magnetic field of the device. Because there is no iron, the magnetic field magnitude, but not the normalized field profile defining the beam focusing (measured by the non-dimensional field index) can be changed by just scaling the currents in all coils by the same factor.

The production of ion beams of various energies is possible in conventional machines, for instance, by installing energy degraders in the beam line [10]. However, this feature comes at the cost of undesirable production of secondary radiation (neutrons and photons) that markedly increases the radiation shielding required for placement in a patient treatment environment. Scaling of the acceleration field intensity permits ion acceleration from the minimum energy permitted by other subsystems of the cyclotron (ion source, RF system, beam extraction system) to the maximum permitted by the coil design. In an iron-free cyclotron, the beam energy can be adjusted continuously by varying the coil system current, Iop(t), as a function of time.
The second operational change when changing the beam energy is the adjustment of the frequency and the amplitude of the RF. For non-relativistic particles, the frequency scales linearly with the field (f ~ B). Other physics issues that must be addressed to accomplish energy variability in conjunction with the magnetic field change are the ion injection and the beam extraction.

The purpose of this study is limited to deriving the scaling laws governing the controlled parameters of the cyclotron magnet including the RF system. Some issues related to the design of a magnet compatible with the proposed method of the beam energy modulation are discussed, mostly from the standpoint of specifying the areas for the future investigations.

2. Scaling Laws

Assume there is a design of a "basic" iron-free synchrocyclotron characterized by a magnetic field profile, $B_0(r)$, and a particle extraction energy, $T(R_{ex}) = T_0$, at the extraction radius, R_{ex}, such that the Lorentz factor is defined as

(1) $\gamma(R_{ex}) = 1 + T_0/E_0$, where $E_0 = m_0c^2$

An iron-free design permits extraction at reduced beam energy,

(2) $T = K_T T_0$,

where $K_T \leq 1$ is the beam energy scaling coefficient.

The basic heavy-ion synchrocyclotron equations [11],

(3) $Am_0\gamma(r)\frac{v(r)^2}{r} = Zev(r)B(r)$, and $\gamma(R_{ex}) = 1/\sqrt{1-[v(r)/c]^2} = 1 + T(r)/E_0$,

yield the magnetic rigidity,

(4) $B(r)r = \frac{Am_0c}{Ze}\sqrt{\gamma(r)^2 - 1}$.

Here *A* and *Z* respectively are the particle atomic number and charge multiple with respect to e, the charge of an electron; m_0 - rest mass of a nucleon; $B(r)$ – magnetic field, $v(r)$ - particle

velocity, both as a function of the radius, r; c - speed of light and $E_0 = m_0 c^2$ - energy of a nucleon.

Equations (3) and (4) result in the following scaling of the magnetic field at the extraction radius,

(5) $$K_B(K_T) = \frac{B(R_{ex},K_T)}{B(R_{ex},1)} = \sqrt{\frac{\gamma(R_{ex},K_T)^2-1}{\gamma(R_{ex},1)^2-1}}, \quad \text{where} \quad \gamma(R_{ex},K_T) = 1 + K_T\frac{T_0}{E_0}$$

where K_B is the magnetic field scaling coefficient. In an iron-free cyclotron the field changes by a proportional change of the coil currents, so that this proportion stays at any radius,

(6) $$B(r,K_T) = K_B(K_T)B(r,1), \quad \text{where} \quad B(r,1) = B_0(r)$$

Due to this linear proportionality the focusing properties defined by a non-dimensional field index,

(7) $$n(r) = -\frac{r}{B(r,K_T)}\frac{dB(r,K_T)}{dr} = -\frac{r}{B_0(r)}\frac{dB_0(r)}{dr}$$

stays the same as in the "basic" design.

Generally speaking, scaling of the frequency and the gain of the beam acceleration system are not unique. Let us consider a scheme, in which the particle is made to follow the same trajectory at any K_T.

Substituting linear velocity by the angular velocity, $v(r) = r\omega(r)$, in (3) we derive

(8) $$\omega(r) = \frac{ZeB(r)}{Am_0\gamma(r)},$$

This means that for a variable energy iron-free design the acceleration frequency shall scale as

(9.a) $$\omega(r,K_T) = K_\omega(r,K_T)\omega(r,1)$$

Substituting (8), (3) and (4) into (9.a) yields an acceleration frequency scaling coefficient, $K_\omega(r,K_T)$, given by:

(9.b) $$K_\omega(r,K_T) = K_B(K_T)\frac{\gamma(r,1)}{\gamma(r,K_T)}, \text{ where } \gamma(r,K_T) = \sqrt{1+\left[K_B(K_T)\frac{B(r,1)rZe}{Am_0c}\right]^2}$$

The acceleration gap voltage, $V(r,K_T)$, has to similarly scale with the local beam energy,

(10.a) $$V(r,K_T) = K_V(r,K_T)V(r,1),$$

where the acceleration voltage scaling coefficient, K_V, is given by:

(10.b) $K_V(r,K_T)=\frac{T(r,K_T)}{T(r,1)}, \qquad T(r,K_T)=E_0[\gamma(r,K_T)-1]$

3. "Basic" Design

Let us consider an H^- (A=Z=1) Iron-free Synchrocyclotron capable of extracting the beam at a variable, up to 250 MeV. Its field profile is designed to be the same as in the k250 syncrocyclotron [2].

General principles of designing iron-free cyclotrons were described in [12]. To reduce the size of the cryostat required for the superconducting coils let us use NbTi Cable in Channel (CIC at B_{max}=5.5 T, j_{wp}=100 A/mm^2) for the Main and Field Shaping coils. Room Temperature (RT) copper Shielding coils are used and are located outside the cryostat.

The coil build, the B-field and beam energy profile as well as focusing characteristics and contours of the fringe fields in the vicinity of the magnet are shown in Figs 3-8. Fig. 3 shows a Vector Fields (VF) Opera model for the coil set. Fig. 4 shows the variation in the cyclotron magnetic field in Tesla with radial position. Fig. 5 shows the variations of the radial betatron tune, ϑ_r, and the axial betatron tune, ϑ_z, with radial position. Fig. 6 shows that weak focusing is in place at all radii up to the extraction point at R_{ex}=0.9049 m, where $\vartheta_r(R_{ex})=2\vartheta_z(R_{ex})$. Fig. 7 shows the variation in beam energy with radial position, while Fig. 8 shows contours of fringe magnetic field with radial and axial position outside of the cyclotron.

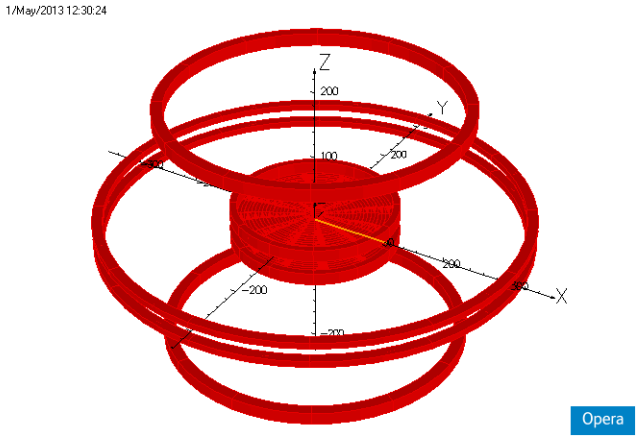

Fig. 3 Opera Model

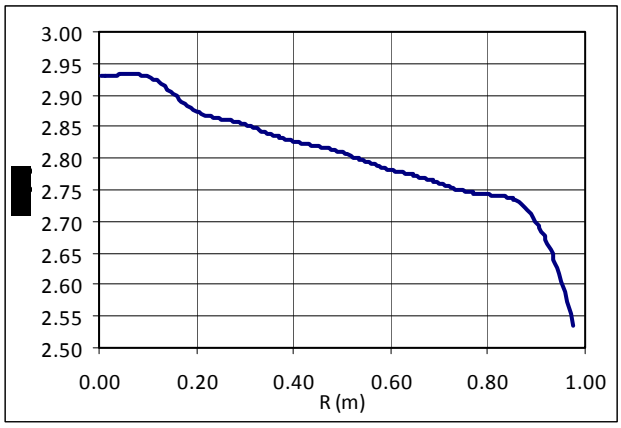

Fig. 4 $B(r)$, T

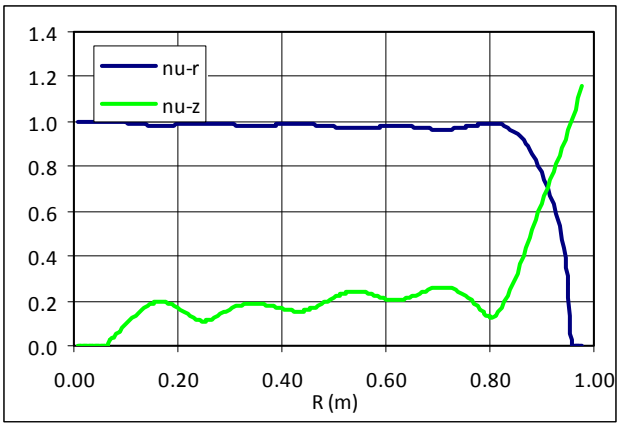

Fig. 5 $\vartheta_r(r)$ and $\vartheta_z(r)$

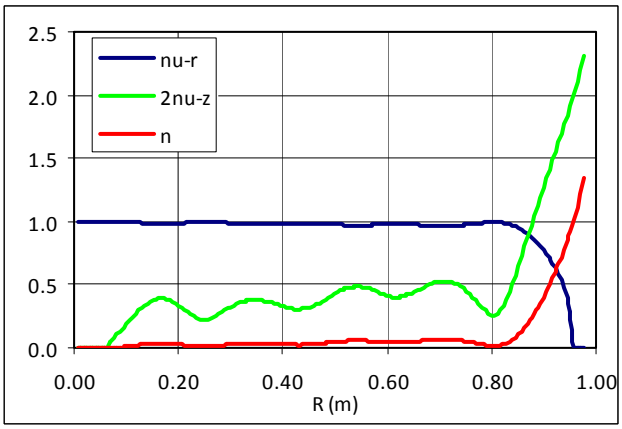

Fig. 6 $n(r), \vartheta_r(r), 2\vartheta_z(r)$

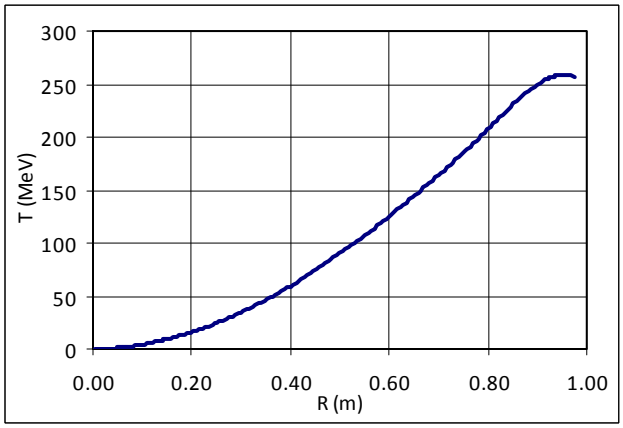

Fig. 7 $T(r)$, MeV

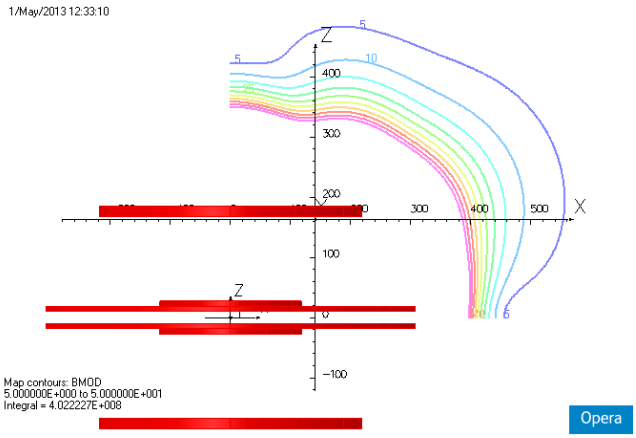

Fig. 8 Contours of Fringe Fields
(10 lines 5 gauss to 50 gauss)

Table 1 summarizes general characteristics of the "basic" magnetic design. Table 2 shows the breakdown of the defining parameters of the coils. The (R1,Z1) and (R3,Z3) locations listed in Table 2 indicate the coordinates of the innermost and outermost (with respect to the center of the machine) corners of the coil envelope.

Table 1 General Characteristics

Beam		
B0	T	2.931
Bex	T	2.704
Rex	M	0.9049
Tex	MeV	252.69
Coil		
E	MJ	21.78
Field		
B(R=5m)	gauss	15
B(Z=5m)	gauss	2

Table 2 Coil Parameters

Coil	R1	Z1	R3	Z3	j_{wp}	NI	Bmax	V	Cond	Dens*	Mass
#	m	m	m	m	A/mm2	A-t	T	m3		kg/m3	kg
1	1.080	0.100	1.180	0.272	100.00	1.72E+06	5.50	0.1222	CIC	8000	978
2	0.130	0.100	0.180	0.106	100.00	3.03E+04	3.36	0.0003	CIC	8000	2
3	0.180	0.100	0.280	0.102	100.00	2.16E+04	3.04	0.0003	CIC	8000	2
4	0.280	0.100	0.380	0.105	100.00	4.54E+04	3.07	0.0009	CIC	8000	8
5	0.380	0.100	0.480	0.105	100.00	4.78E+04	2.98	0.0013	CIC	8000	10
6	0.480	0.100	0.580	0.106	100.00	6.19E+04	3.00	0.0021	CIC	8000	16
7	0.580	0.110	0.680	0.118	100.00	7.79E+04	3.22	0.0031	CIC	8000	25
8	0.680	0.110	0.780	0.119	100.00	9.44E+04	3.07	0.0043	CIC	8000	35
9	0.780	0.110	0.880	0.119	100.00	8.55E+04	2.97	0.0045	CIC	8000	36
10	0.880	0.100	0.980	0.110	100.00	9.67E+04	3.12	0.0056	CIC	8000	45
11	0.980	0.100	1.080	0.101	100.00	1.30E+04	3.90	0.0008	CIC	8000	7
12	2.021	1.673	2.180	1.855	-10.00	-2.89E+05	na	0.3814	Cu	7200	2,746
13	2.927	0.100	3.073	0.187	-10.00	-1.27E+05	na	0.2400	Cu	7200	1,728
Total (all 26 coils)									CIC		2,328
									Cu		8,949
									All		11,277

* Basic material density of Copper coils was reduced from 9000 kg/m3 by a factor of 0.8. This factor accounts for the water channel in the copper coils. This is a very rough scaling and it has to be adjusted for the actual conductor design.
** The weight of CIC includes both the Channel stabilizer and the NbTi superconductor. The weights in the table are good only for benchmarking the system design. For the pricing purposes the weights of the channel and of the Superconducting (SC) cable have to be reevaluated for a specific design of the conductor. Here the Channel is assumed to be made of copper. Aluminum channel can be used to reduce the weight and the cost of the system.

The cryostat encloses coils #1 thru coil #10, the outermost of which extends to R = 1.18 m radially and to Z = +/-0.27 m axially. The cryostat has an outer diameter of 2.5 m and a height of 0.7 m, with an inner diameter, D < 16 cm, axial bore for the External Ion Source and 10-cm high mid-plane tunnels for the beam acceleration (inflector, RF, and stripper) equipment. The weight of the cryostat and the coil support structure is not accounted for in Table 2 but it is not expected to be more than 2,500 kg.

4. Beam Energy Modulation

Let us use the requirements to the beam energy/range modulation for the proton radiotherapy as defined in [12] is 2 MeV steps for protons (~0.25 cm step in range) at a ~100 millisec step rate.

For a 250 MeV proton cyclotron this means that that the beam energy, *T*, to treat a tumor extending through a depth of 30 cm, shall be linearly reduced from T_0=252.69 MeV to zero in 12.6 seconds at a rate of 20 MeV/s.

The governing equations as a function of time are (1)-(10) where

(10) $K_T(t) = 1 - t/12.6, \qquad K_B(t) = 0.938\sqrt{K_T(t)(1 + 0.1343K_T(t))^2}$

The variation in stored magnetic energy, $E_m(t)$, is given by:

(11) $Em(t) = K_B(t)Em(0),$

where $Em(0)$=21.78 MJ is the maximum stored electro-magnetic (EM) energy of the system at t=0.

The following diagrams illustrate the variation of the characteristics of the magnetic system as a function of time.

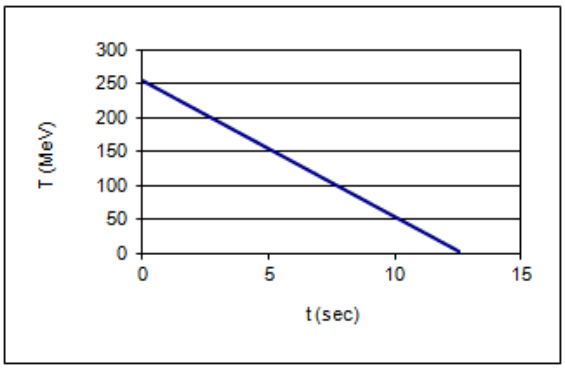

Fig. 9 Beam energy vs. time

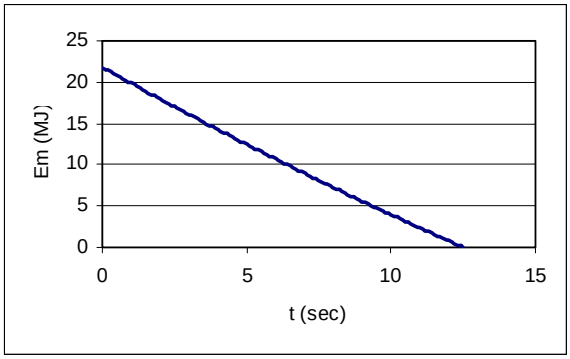

Fig. 10 EM energy vs. time

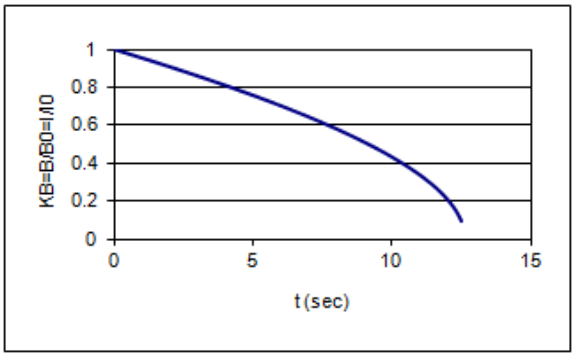

Fig. 11 Field/Coil Current Scaling coefficient vs. time

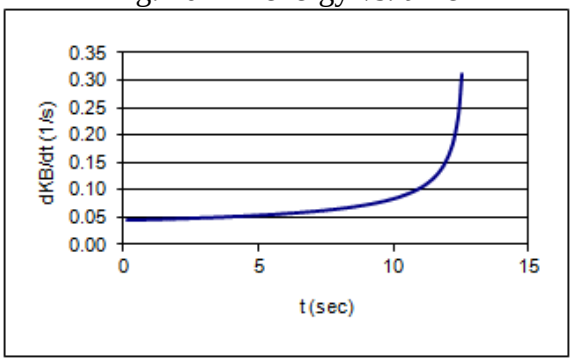

Fig. 12 dK_B/dt vs. time

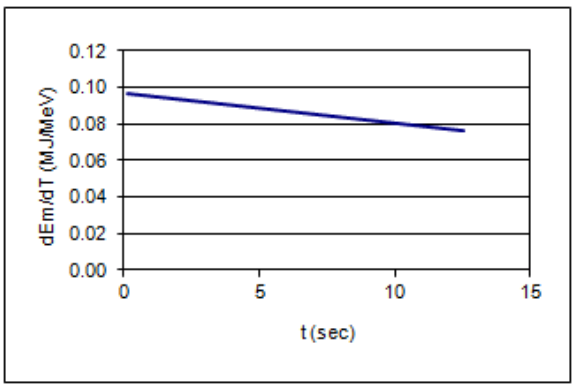

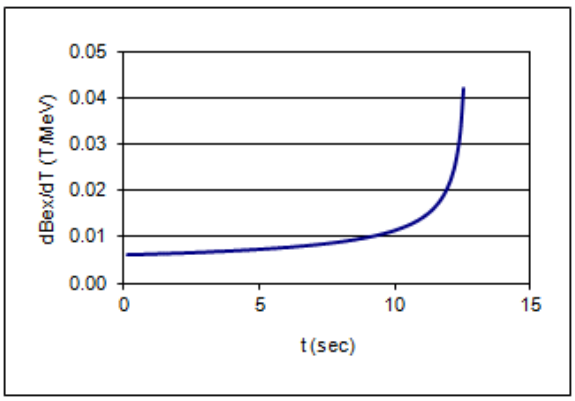

Fig. 13 dEm/dT vs. time

Fig. 14 dB_{ex}/dT vs. time

Assume that all coils are in series, driven by the same power supply and $Iop(0) = 2$ kA. Then the terminal voltage, $V_m(t)$, will vary as

(12) $Vm(t) = Pm(t)/Iop(t))$, where $Pm(t) = dEm(t)/dt$

The power, $Pm(t)$, and the terminal voltage, $Vm(t)$, are shown in Figs. 15-16 as functions of time. Note that most of the time the voltage is about 1 - 2 kV and only at the very end it grows to 10 kV. It may well be that Proton Radiotherapy at such small energies will use different Energy/Range modulation regimes.

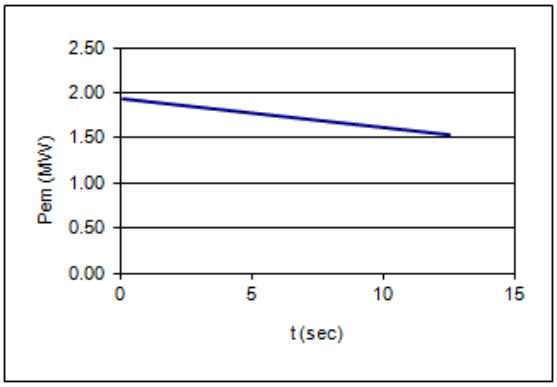

Fig. 15 EM Power vs. time

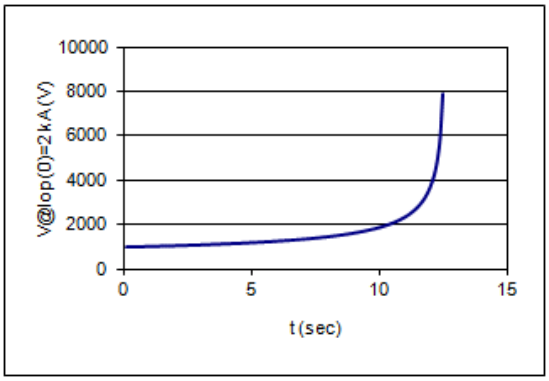

Fig. 16 Terminal Voltage (@Iop(0)=2 kA) vs. time

The terminal voltage is calculated for the total EM energy of the system including both RT and SC magnets. Both energy and voltages at the terminals of the SC magnet will be lower. Table 3 shows an inductance matrix calculated for the turn numbers corresponding to $Iop(0) = 2$ kA.

Table 3. Inductance matrix @ $Iop(0) = 2$ kA

i	j	L_{ij} (H)
1	1	1.1160E+01
1	2	5.0067E-01
2	2	7.2566E-01

Here Coil 1 and Coil 2 represent combined SC and RT coils, respectively. Respective EM energy of SC and RT coils is 21.32 MJ and 0.45 MJ. This means that maximum voltages at the terminals of the SC coil will scale from those in Fig. 16 by an insignificant factor of 21.32/21.78=0.98, i.e. will be just 2% lower.

Figures 17 and 18 depict the time variation of the primary RF characteristics, the frequency scaling coefficient, $K_\omega(R_{ex})$, and the gap voltage coefficient, $K_V(R_{ex})$. Values of both coefficients are taken at the extraction radius.

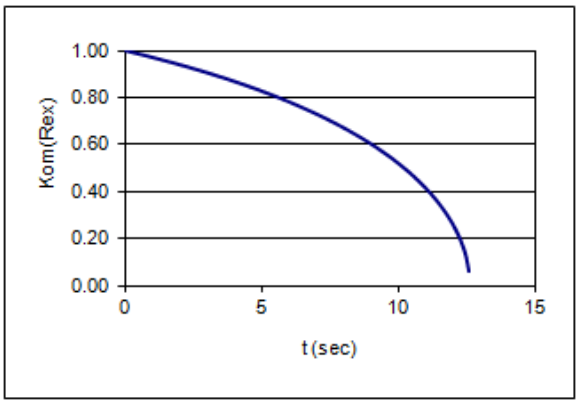

Fig. 17 $K_\omega(R_{ex})$ vs. time

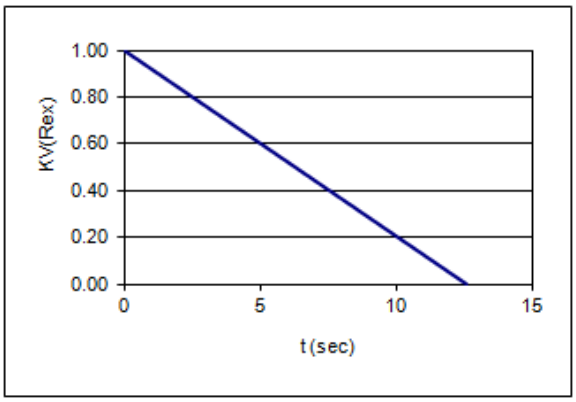

Fig. 18 $K_V(R_{ex})$ vs. time

The variation of the coefficients as a function of the radius is shown in Fig. 19 for the maximum beam energy (K_T=1 @ t=0).

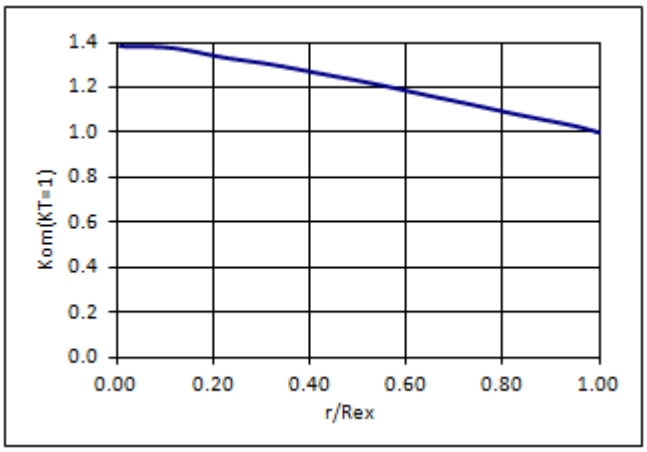

Fig. 19 $K_\omega(K_T = 1)$ vs. r/R_{ex}

5. Beam Extraction

Beam extraction from a variable energy iron-free synchrocyclotron can be accomplished using any of the conventional schemes. The same as above principle of using the same stationary hardware arrangement and scaling the controlled parameters with the beam energy can be utilized.

5.1 Extraction by Stripping

The simplest extraction scheme may be by using a stripper permanently installed at Rex.

At the extraction the momentum,

(13) $p(R_{ex}, K_T) = m(R_{ex}, K_T) * v(R_{ex}, K_T) = K_B(K_T) * p(R_{ex}, 1),$

scales the same way as $B(r, K_T)$, i.e. is proportional to $K_B(K_T)$

Since in general terms

(14) $mvdv/dx \sim evB$

it follows that $(dv/dx)/v \sim (eB)/(mv) \sim (eK_B B_0)/(K_B p_0) \sim (eB_0)/p_0$

and the shape of the trajectory is independent of the extraction beam energy.

Let us check the extraction trajectory independence of the beam energy using VF Opera modeling. If the above theory is correct, protons with properly scaled energy launched at the same spot into the properly scaled magnetic field shall follow the same path. Note that VF Opera Reference Manual claims that "the TRACK command calculates the trajectories of charged particles through the electric and/or magnetic fields (including full relativistic correction)…".

Table 4 and Fig. 20 show scaling of the magnetic field generated by scaling the current density in the COND file as a function of the beam extraction energy, T, scaled in increments of 0.2 from $T = T_0$ to $T = 0$.

Table 4. Scaling of Beam Energy/Magnetic Field Modulation

K_T=T/T_0	T	γ	Rigidity	B_{ex}	K_B=B/B_0	Em	j_{sc}	j_{cu}
	MeV		T*m	T		MJ	A/cm^2	A/cm^2
1.0	252.6939	1.26932	2.44675	2.704	1.0000	21.78	10000.00	1000.00
0.8	202.1551	1.21545	2.16231	2.390	0.8837	20.47	8837.49	883.75
0.6	151.6163	1.16159	1.84971	2.044	0.7560	18.94	7559.88	755.99
0.4	101.0776	1.10773	1.49135	1.648	0.6095	17.00	6095.22	609.52
0.2	50.53878	1.05386	1.04098	1.150	0.4255	14.21	4254.54	425.45
0.0	0	1.00000	0.00000	0.000	0.0000	0.00	0.00	0.00

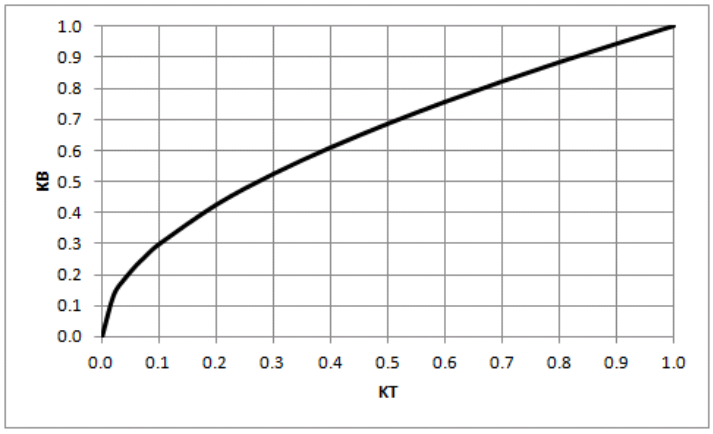

Fig. 20 $K_B(K_T)$ for a sample 250-MeV iron-free design

Five models were analyzed, each having the same coil geometry but different coil current density corresponding to T/T_0=1.0, 0.8, 0.6, 0.4 and 0.2. A proton was launched from the spots with the same X- and Y- coordinates at R_{ex}=90.49 cm with the respective energy, T. To distinguish between the trajectories the initial spots were spaced axially in the Z-direction by 1 mm.

Figures 21.a and 21.b show the trajectories of the proton in the axial and isometric perspectives. They overlay on the axial view but are visibly separated on the isometric view.

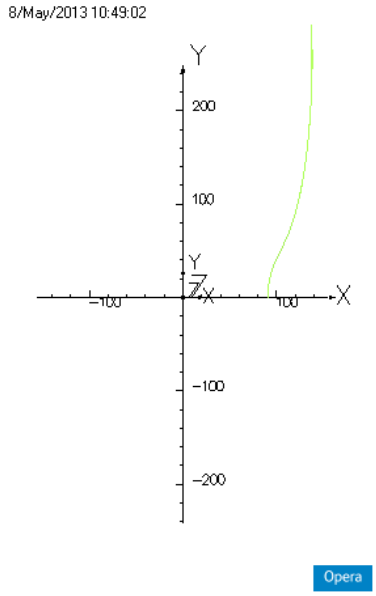

Fig. 21.a Extraction Trajectories, Axial View

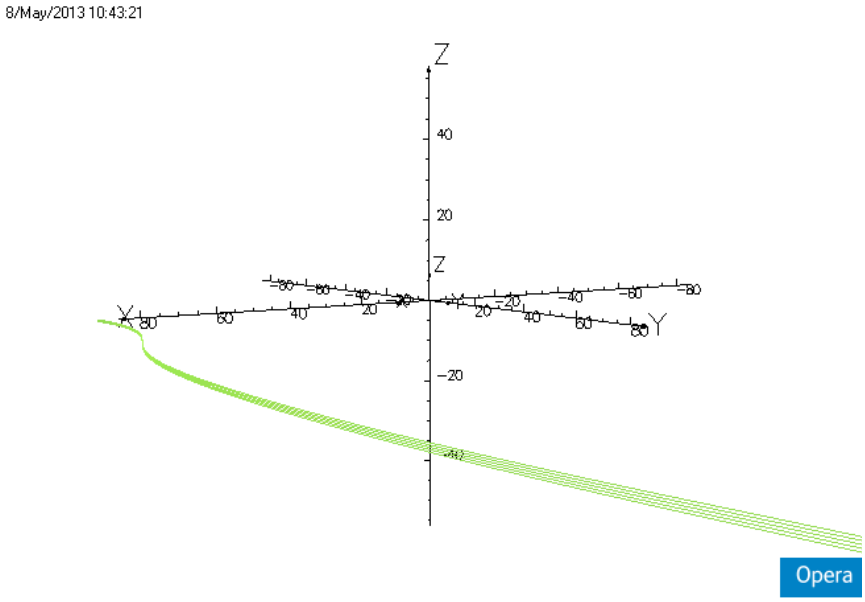

Fig. 21.b Extraction Trajectories, Isometric View

This confirms the above conclusion that for a properly scaled coil current matching the scaled beam energy the trajectories of the particle are the same.

5.2 Regenerative Extraction

The above property opens the opportunity of using regenerative extraction by magnetic bumps generated by small coils changing the current scaled with the same proportion as in the Main/Shaping/Shielding coils. The consequence of this feature is that the design may no longer be limited by using stripping for extraction. Protons can be used instead of H- , which removes the field limitation [13], B < 3 T.

Compact high, ~ 9 T, field proton synchrocyclotron with regenerative extraction and variable currents in Main/Shaping/Shielding/Extraction coils may be a viable design. This would permit reducing the weight of the cyclotron to about 4 tons with the overall dimensions of about 2 m. These weight and dimensions facilitate installing a variable beam energy iron-free cyclotron on a rotating gantry.

6. Discussion

The “basic” magnet design for an iron-free synchrocyclotron was described in Section 3. In this section we discuss the technical issues related to this coil arrangement and the magnet functionality required to accomplish the variable beam energy feature.

The Field Shaping coils were generated under the assumption that their current density j=const, and the axial build is defined by Z1=const and (Z3)=var. The coils can be reoptimized with (Z1, Z3)=const and (j)=var. In the first case the tops of the coils form steps, which may be inconvenient both for manufacturing and for the EM force containment. In the second case the coils can be wound as one or more double pancakes with a variable pitch, which will be accomplished by spacers between the turns.

At r<6 cm the field profile fails the axial focusing condition. This can be easily fixed either by electrostatic focusing or by adding a small copper coil in the RT bore around the External Beam source.

The Main and the Field Shaping coils are offset axially from the midplane by 10 cm. This is expected to be sufficient to accommodate the 5 cm beam space (adding up to 10 cm around the midplane), so that another 5 cm are left for the thickness of the cryostat, thermal insulation, radiation shields and coil support structure. If necessary the offset can be increased, which will result in a slightly higher weight of the conductor and EM energy. In this case, the field profile, B(r), will get smoother.

Transient analyses performed in Section 4 indicate that it is possible to drive the coil energy following the required current versus time scenario using an external power supply or resistor without excessive terminal voltage. Technical implementation of the current dump is to be addressed by more detailed studies. We need to pay special attention to eddy current heating and temperature ratcheting in the cold mass during design of the conductor and the coil cooling scheme.

The maximum peak field of 5.5 T at the ID of the Main Coil wound with the NbTi conductor at current density of 100 A/mm^2 allows a design with a significant temperature margin. More analyses will show if it is sufficient to sustain the AC losses related to the field variation. Using dK_B/dt = 0.05 at the highest field of B_0=5.5 T at t=0 we can conclude that the initial ramp rate of the field decay is 0.275 T/s. This is orders of magnitude less that used for ITER cable tests in PTF [14].

Quench protection of this, multiple-coil, system may present a challenge. However, this task is not expected to be much more difficult than protecting conventional multiple-coil MRI magnets [7].

These comments have no intention of downplaying potential technical difficulties of implementing the variable energy iron-free cyclotron design, but rather aim at defining the areas of research required for its successful accomplishment.

References

1. US Patent 7541905, T. Antaya, et al., High-field superconducting synchrocyclotron

2. A. Radovinsky, “Baseline Magnetic Design, k250z3n-4mu-b1,” K250 project memo, MIT-Plasma Science and Fusion Center, Cambridge, MA, Nov. 27, 2007.

3. US Patent 4,943,781, Martin N. Wilson, Martin F. Finlan, Cyclotron with yokeless superconducting magnet

4. K. M.Subotic: Multipurpose Superconducting Cyclotron,IEEE SC 1984 Proceedings of X International Conference on Cyclotrons and Their Applications, East Lansing 1984, 469-471.

5. Hiroshi Ueda, et al, “Conceptual Design of Next Generation HTS Cyclotron,” in IEEE Transactions on Superconductivity, Vol. 23, No.13 (2013)

6. L. Bromberg, et al, “Ultra-Light ,Magnetically Shielded, High-Current, Compact Cyclotron,” US Patent Application, mit-16121, 26 July, 2013

7. Y. Lvovsky, et al. “Novel technologies and configurations of superconducting magnets for MRI,” Supercond. Sci. Technol. v. 26, 2013

8. www.mevion.com

9. Workshop on Ion Beam Therapy. Summary Report, Bethesda, MD, January 9-11, 2013

10. Y. Jongen, et al. “Current Status of the IBA C400 Cyclotron Project for Hadron Therapy,” Proceedings of EPAC08, Genoa, Italy, 2008, p. 1806

11. Y. Jongen and S. Zaremba, “Cyclotron Magnet Calculations”, CERN 96-02, pp. 139-151. THPAN056Proceedings of PAC07, Albuquerque, New Mexico, USA

12. Carol Johnstone, “Advances Accelerator Technologies for Ion Therapy”, Joint Symposium 2013 on Carbon Ion radiotherapy, May 2-3 2013, Rochester Minnesota

13. R. Baartman, “Intensity limitations in Compact H-Cyclotrons”. Proc. XIV Cycl. Conf. (1995)

14. B. Smith, et al. "A Pulsed Magnetic Field Test Facility for Conductors and Joints," IEEE Trans. Magnetics, vol. 32, pp. 2292-2295, July 1996.